Multi-scale Turbulence Measurement in the Aquatron Laboratory
Project number 300-231: Final Report

submitted to

Nova Scotia Offshore Energy Research Association

by

Alex E. Hay, Maricarmen Guerra-Paris, Tristan Guest, Richard Cheel and Grace Watts
Department of Oceanography, Dalhousie University,

23 July 2019

1 Introduction

This project had two primary objectives: (1) to characterize the flow and turbulence in the Aquatron pool tank, using turbulence sensors calibrated against a traceable standard; and (2) to use this facility to test technologies currently under development for investigating the horizontal variability of turbulence in real-world tidal channels.

The project was motivated in part by the need, in studies of turbine-turbulence-animal interactions in the Aquatron being carried out by other investigators, for quantitative knowledge of turbulence scales and intensity in the Aquatron facility. This knowledge is essential for such studies to have application at the field scale. The project was also motivated by the ongoing studies by the Ocean Acoustics Laboratory at Dalhousie of the use of acoustic remote sensing technologies for turbulence measurement, and in particular validating the acoustic measurements against a laboratory-traceable standard. The third motivation was to contribute to the development of new approaches to the measurement of large-eddy turbulence in the field.

The project was carried out in two stages. The first stage was a 1-week experiment in January 2019, in which the flow in the Aquatron pool tank was characterized at turbulence-resolving scales using a Nortek Signature1000 5-beam acoustic Doppler current profiler (ADCP). The results from this experiment are summarized in the Interim Report for the project. A principal result was that the estimates from the ADCP of the rate of dissipation of turbulent kinetic energy were very high – $O(10^{-2})$ kg/m^3 – but too scattered to confirm the expected cubic dependence on mean flow speed. A second result was that the mean flow exhibited the behaviour of a neutrally buoyant turbulent jet discharged from a circular nozzle, but constrained from above by the free surface, so that the maximum axial velocity in the jet far-field fell off more slowly with distance x from the nozzle than the $1/x$ dependence expected for a free jet.

The second stage of the project involved a second experiment, carried out over a two week

period in April 2019. In addition to the ADCP, measurements were made with an new instrument – the MicroRider – which had been received from the manufacturer in March. The MicroRider carries two laboratory-calibrated shear probes for measuring velocity fluctuations in turbulent flows. The primary goal of the second stage was to compare the dissipation rate estimates obtained with the MicroRider to those from the ADCP. A second goal was to measure the larger-scale turbulence and flow field using video-tracked surface drifters.

2 Instruments and Methods

The instrument locations and data collection protocols on each day of the experiment are summarized in Table 1. Figure 1 is a sketch of the layout in in the Aquatron pool tank. The instrumentation setup is documented in Figures 2 and 3. Measurements were made at different nozzle discharges with all four pumps operating, usually from 50% to 100% of maximum in 10% increments. The nozzle is 40 cm in diameter, with its centre located at 0.5 m depth. The positions occupied by the different instruments along the jet axis, relative to the profiles of maximum axial velocity, are summarized in Figure 4.

It is important to note that the ADCP – when deployed on the tank bottom – was usually operated with only beams 3 and 5 active. As indicated by the sketch in Fig. 5, beam 5 is vertical, and so measures the vertical component of velocity, w, whereas beam 3 is slanted away from vertical. The ADCP frame was oriented such that beam 3 was in line with the jet centreline, and directed toward the nozzle. The beam 3 velocities therefore included contributions from both w and the axial velocity component, u. The value of u was determined from the beam 3 and 5 velocities geometrically, using the 25 degree beam 3 slant angle. The ADCP frame was deployed such that beam 5 was as close as possible to the MicroRider without getting a reflection from it (Fig. 3). Beam 1 would have "seen" the MicroRider pressure case, and so was not activated. The orthogonal beam pair, 2 and 4, were not activated because the mean

transverse velocity is of opposite sign on either side of the jet. The ADCP acquired data in 20 cm range cells at 8 Hz, except for one set of tests when a 16 Hz sample rate was used (Table 1).

The MicroRider carries two shear probes (Fig. 5) which are expected to yield two independent, but equal, estimates of the dissipation rate. However, the dissipation rates estimated from first pair of probes – used on yd100 and 101 (Table 1) – were different from each other, so replacement probes were installed on yd 102. The dissipation estimates obtained with the two replacement probes were in good agreement. The first pair of probes were sent to the manufacturer after the experiment. After the experiment, the initial set of probes was returned to the manufacturer and replaced under warranty. Overall, the data from the MicroRider were of very high quality, and free of contamination from vibration, owing to the rigid mount to the bridge (Fig. 2) and the stream-lined underwater and surface-piercing supports (Figs. 2 and 6). The shear probes were sampled at 2048 Hz.

The MicroRider and ADCP were both hardwired to a data acquisition and control station on the apron surrounding the pool tank. The connection to the bottom-mounted ADCP was via an underwater cable running along the bottom of the tank. Above-water cables running along the bridge were used for the MicroRider and the ADCP when it was mounted in the horizontal orientation (Fig. 2). Data were recorded for 20 minutes at each discharge.

The cork surface drifters (Fig. 3) were released in batches of ca. 300 corks, with two people strewing the corks by hand on either side of the jet centreline within a meter or two of the nozzle. The corks were monitored with two digital video cameras mounted to the ceiling (Fig. 1). The two video data streams were recorded at a frame rate of 25 Hz and 1640×1232 resolution on separate Raspberry Pi computers synchronized via a wireless link to a master Linux PC. The corks were collected with dip nets when they reached the pool tank wall, and the process repeated, usually 3 to 4 times for each discharge.

The vorticity drifter (Fig. 3) was equipped with a 9-axis inertial motion unit. It was deployed

at the same time as some of the cork drifter releases.

3 Main Results

3.1 Horizontal Profiles of Axial Mean Velocity

The variation of the mean jet axial velocity, U, with horizontal along-axis position, x, at 0.5 m depth is shown in Figure 7 as a function of discharge percentage. These results were obtained with the ADCP mounted horizontally to the bridge and aimed toward the nozzle (Fig.2). The profiles exhibit the behaviour expected of a neutrally-buoyant jet discharged from a circular nozzle, adjacent to a boundary (the free surface here): i.e., the maximum velocity is nearly independent of x in the near-field ($x/D < 7$), and falls off as $x^{-0.7}$ in the far-field. Thus, these results confirm the behaviour indicated by data from the January experiment but, being continuous in space, represent a considerable improvement over the January results, which were based on bottom-mounted ADCP at discrete positions along the jet axis.

3.2 Vertical Profiles of Mean Velocity

Vertical profiles of mean axial velocity, u, and mean vertical velocity, w, are plotted in Fig. 8 as a function of discharge. These profiles are from the bottom-mounted ADCP on yd100 when it was positioned at $x = -1.07$ m (Table 1). The velocity maximum is between 0.5 and 1 m below the surface, consistent with the 0.5 m depth of the nozzle. The maximum velocities increased from about 0.8 m/s at 50% of maximum discharge to about 1.6 m/s at 100%. The jet thickness scale is about 1 m.

It is worth revisiting the top panel in Fig. 4 at this point, from which it can be seen that the beam 3 and 5 range bins at the 0.5 m depth of the MicroRider are separated by about 1.3 m horizontally. Thus, the u profiles in Fig. 8 represent a spatial average over this interval and, since the the axial velocities (measured by the ADCP when it was in its horizontal position) are

approximately linear at this separation, the u profiles represent the flow at $x \sim -1.4$ m.

Note as well that the segments of these profiles immediately below the water surface are unreliable, because the beam 3 data in this region are contaminated by the surface reflection, detected via side-lobes in the transducer beam pattern. Given the 3 m vertical range to the surface, and the 25 degree slant angle for beam 3, the velocities in Fig. 8 beyond $z \sim 2.7$ m are unreliable. Below this z level, the velocity maxima are well-defined.

3.3 Frequency Spectra

Figure 9 shows the beam 3 and 5 velocity spectra in the range cells corresponding to the velocity maxima on yd100. The noise levels at low flow are consistent with the values expected from the manufacturer's instrument setup software. Subtracting the noise floor reveals the -5/3 dependence expected in the inertial subrange. Figure 10 shows the spectra from the MicroRider. The spectra are remarkably free of noise, very similar for the two probes, and exhibit a broad -5/3 range.

3.4 Wavenumber Spectra

The frequency spectra were converted to (cyclic) wavenumber spectra by invoking Taylor's frozen turbulence hypothesis, which requires specifying the mean flow speed, U. The MicroRider is equipped with an electromagnetic flowmeter mounted in the nose of the instrument (Fig. 5), specifically for this purpose. However, the values of U from this sensor did not exhibit the expected linear dependence on discharge, whereas those from the horizontal ADCP did (Figure 11). Similarly, because of the spatial separation between beams 3 and 5, the values of U from bottom-mounted ADCP were not representative of the mean flow at either the beam 3 or beam 5 range cell locations. Consequently, both the MicroRider and the ADCP frequency spectra were transformed to wavenumber spectra using U from the horizontal ADCP.

Figure 12 shows the wavenumber spectra from the two instruments. The ADCP spectra are for the beam 5 range cell at the depth of the MicroRider on yd106: i.e., at the x position occupied by the MicroRider shear probes the previous day (Table 1). Note the tendency for the ADCP spectra to fall off more steeply than -5/3. Note also the tendency for both sets of spectra to level off and/or peak in the vicinity of 2 cycles/m, indicating that production of turbulent kinetic energy occurred at spatial scales in the vicinity of 0.5 m. This scale nicely corresponds to the widths of the zones of high mean shear above and below the velocity maximum (Fig.8).

3.5 Dissipation

Figure 13 shows the dissipation rates at 0.5 m depth determined from the MicroRider and ADCP wavenumber spectra, plotted versus the mean flow speed as measured by the horizontal ADCP. The expected dependence of ϵ on U^3 is exhibited clearly by both data sets. The MicroRider estimates are a factor of 3 higher.

A possible contributor to the factor of 3 difference is the uncertainty in the mean velocity estimates. Uncertainty in U affects the ADCP ϵ estimates linearly, whereas the MicroRider estimates are function of U^{-4} (*1*). For the ADCP, the uncertainty is mainly due to high mean shear across the jet in the vertical (Fig.8) and in the horizontal (which is presumably similar). For the shear probes, the uncertainty in U similarly depends on the position of the shear probes relative to velocity maximum in the jet.

However, the steeper than -5/3 rolloff exhibited by the ADCP wavenumber spectra in Fig. 12 suggests that spatial averaging of the velocity fluctuations within the ADCP range cells must contribute to the difference.

3.6 Drifters

Figures 14 and 15 show the results from one set of cork releases at maximum discharge. The breaks in the drifter tracks are the result of occasional failures by the image processing algorithm to detect the corks. These data illustrate entrainment of passive tracers into the jet at the surface in the jet near-field, and the tendency for the surface speeds to increase with increasing distance from the nozzle in the near-field, as expected for a submerged jet. The Figure 16 shows the u velocities averaged in 30×30 cm bins along and transverse to the jet axis. The mean axial speed increases linearly with distance from the nozzle to values approaching 0.5 m/s at $x = 4$ m: i.e., less than the maximum speed in the jet at depth, and consistent with the tendency exhibited by the vertical profiles in Fig. 8 for $U(z)$ to decrease toward the surface. The transverse profile at $x = 3$ m, though noisy, indicates a value of about 1 m for the width of the jet. The axis of the jet is located, not at $y = 0$, but at a negative y value. As indicated in plan view (Figs. 14 and 15) the jet axis was directed to the right of the $y = 0$ line during this run. This effect is evidence of the previously mentioned tendency of the jet to wander laterally, in response to its intrinsic shear instability coupled to the natural modes of circulation in the circular tank.

An example data set from the Vorticity Drifter is shown in Fig. 17. Two time series are shown: one is the vorticity determined from the 9-axis IMU onboard the drifter; the other is the vorticity estimated from the overhead video imagery. The two time series are very similar in the first 40 seconds of the record, the rotation rates having both the same magnitude and the same sign (note the rotation direction reversal at 25 s). The agreement is not good in the 40 to 50 s interval, when the rotation rate was much higher, possibly because the video-based measurements are – so far – proving to be more difficult to determine at high rotation rates. This is work in progress.

4 Summary

The objectives of the project were all successfully completed. In particular:

- the vertical structure of the mean flow was measured as a function of along-axis position and nozzle discharge, demonstrating pronounced vertical shear above and below the velocity maximum at ca. 0.7 m depth;

- the maximum axial velocity is approximately constant in the jet near-field ($x/D < 7$), and falls off in proportion to $x^{-0.7}$ in the far-field, consistent with the behaviour expected of a neutrally buoyant jet discharged from a round nozzle adjacent to a boundary (the free surface in this case);

- estimates of turbulent kinetic energy dissipation rate, ϵ, were obtained at a depth of 0.5 m both remotely, using a state-of-the-art 5-beam acoustic Doppler profiler, and directly using shear probe sensors traceable to a laboratory standard;

- both the remote and direct measurements of ϵ exhibit the expected dependence on U^3;

- the remote acoustic measurements of ϵ were consistently lower than the direct measurements, by a factor of 3;

- the factor of 3 difference might be due in part to the uncertainties in the mean speed estimates arising from the high mean shear across the jet, but the steeper than -5/3 rolloff exhibited by the ADCP spectra in the inertial subrange points to spatial averaging within the ADCP range cells;

- the trajectories extracted from the video-tracked drifters mapped the recirculation and entrainment in the jet near-field, and axial acceleration of the surface flow in the nearfield/farfield transition region;

- the angular rotation rates registered by the 9-axis IMU on the Vorticity Drifter are in promising agreement with estimates from the video imagery, indicating that the approach should prove useful for vorticity measurements in the field.

The dissipation rates in the immediate far-field of the jet, where maximum mean axial velocities were between 0.6 and 1.6 m/s, ranged from 2×10^{-3} to nearly 0.1 W/kg. These values are two to three orders of magnitude higher than those observed in Grand Passage at higher (2 to 3 m/s) mean flow speeds (*2*). In Minas Passage, values approaching 1×10^{-3} W/kg have been observed at 3 m/s mean flow speeds (*3*). Dissipation rates in the Aquatron are higher than those in the field, despite the lower mean flow speeds, likely because of turbulence production at the pumps, in the conduits leading to the nozzle, and in the envelope of high mean shear around the jet axis.

Acknowledgements

The authors thank Justine McMillan, Peter Stern and Rolf Lueck (Rockland Scientific International) for their assistance and advice regarding the MicroRider setup and analysis of the shear probe data, Greg Trowse (Luna Ocean) for assistance with the development of the vorticity drifter; and Jim Eddington (Aquatron) for his skilled operation of the discharge system and technical support during the experiment.

References

1. L. Merckelbach, A. Berger, G. Krahmann, M. Dengler, J. R. Carpenter, *Journal of Atmospheric and Oceanic Technology* **36**, 281 (2019).

2. J. M. McMillan, A. E. Hay, *Journal of Atmospheric and Oceanic Technology* **34**, 5 (2017).

3. T. H. E. Clark, *et al.*, *European Wave and Tidal Energy Conference* (Cork, Ireland, 2017).

YD[†]	Discharge	ADCP				MicroRider		
	(%)	Depth (m)	$x_5{}^{a*}$ (m)	$x_3{}^{a*}$ (m)	beams	Depth (m)	x^* (m)	Shear Probes
100	50:10:100	3.23	-0.77	-1.96	3 and 5	0.5	-0.1	1984,1983
101[b]	70:10:100	3.08	0.26	-0.88	3 and 5	0.5	-0.1	1984,1983
101	50,60	3.08	0.26	-0.88	5 only[c]	0.5	-0.1	1984,1983[d]
102	50:10:100	3.26	-0.76	-2.00	3 and 5	0.5	-0.1	1982,1981[e]
105[f]	50:10:100	2.54	-2.60	-3.53	5 only	0.5	-0.1	1982,1981
105	50:10:100	2.54	-2.60	-3.53	3 and 5	0.5	-1.72	1982,1981
106	100:-10:50	2.81	-1.70	-2.76	3 and 5	NA	NA	NA
108[g]	50:10:100	0.5	0.53	NA	5 only	NA	NA	NA

[†] YD stands for yearday, with January 1 being YD1

[*] measured relative to the position of the MicroRider endcap on yd100, ~ 5.1 m from nozzle

[a] corrected for pitch

[b] Cork drifter runs

[c] 16 Hz sample rate, otherwise the ADCP sample rate was 8 Hz

[d] rotated shear probes

[e] replaced shear probes

[f] ADCP HR mode tests

[g] Horizontal ADCP

Table 1: Data Collection Summary

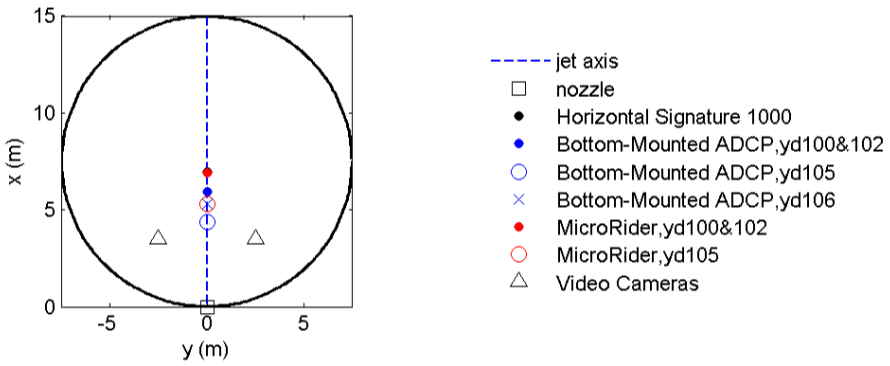

Figure 1: Plan view sketch of the pool tank showing sensor positions.

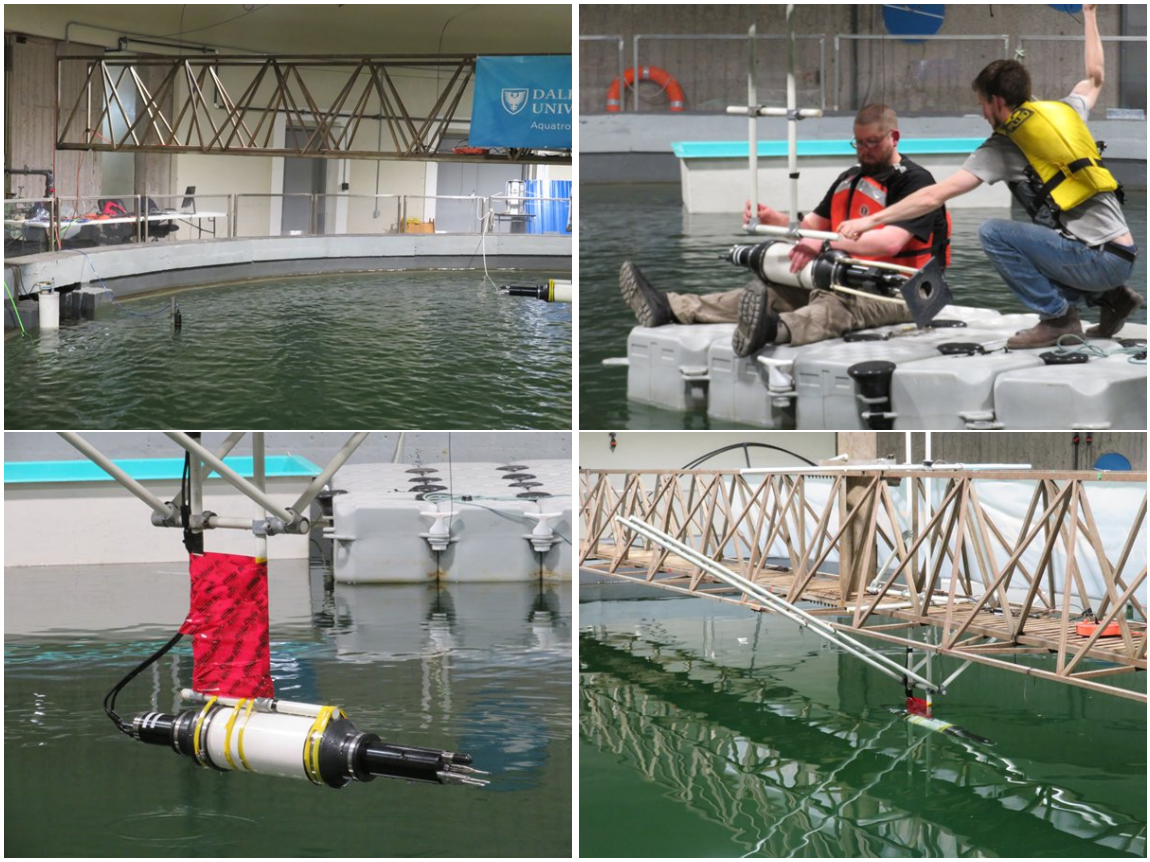

Figure 2: Top left: the pool tank with the bridge in raised position. The Vectrino is at left, ca 1 m in front of the discharge nozzle (not visible). The MicroRider is at right. Top right: Richard Cheel and Tristan Guest mounting the MicroRider to its support. Bottom left: The MicroRider on its support frame. The red tape is a low-cost fairing. Bottom right: the bridge in its lowered position, with the MicroRider immersed at 0.5 m depth, and no flow.

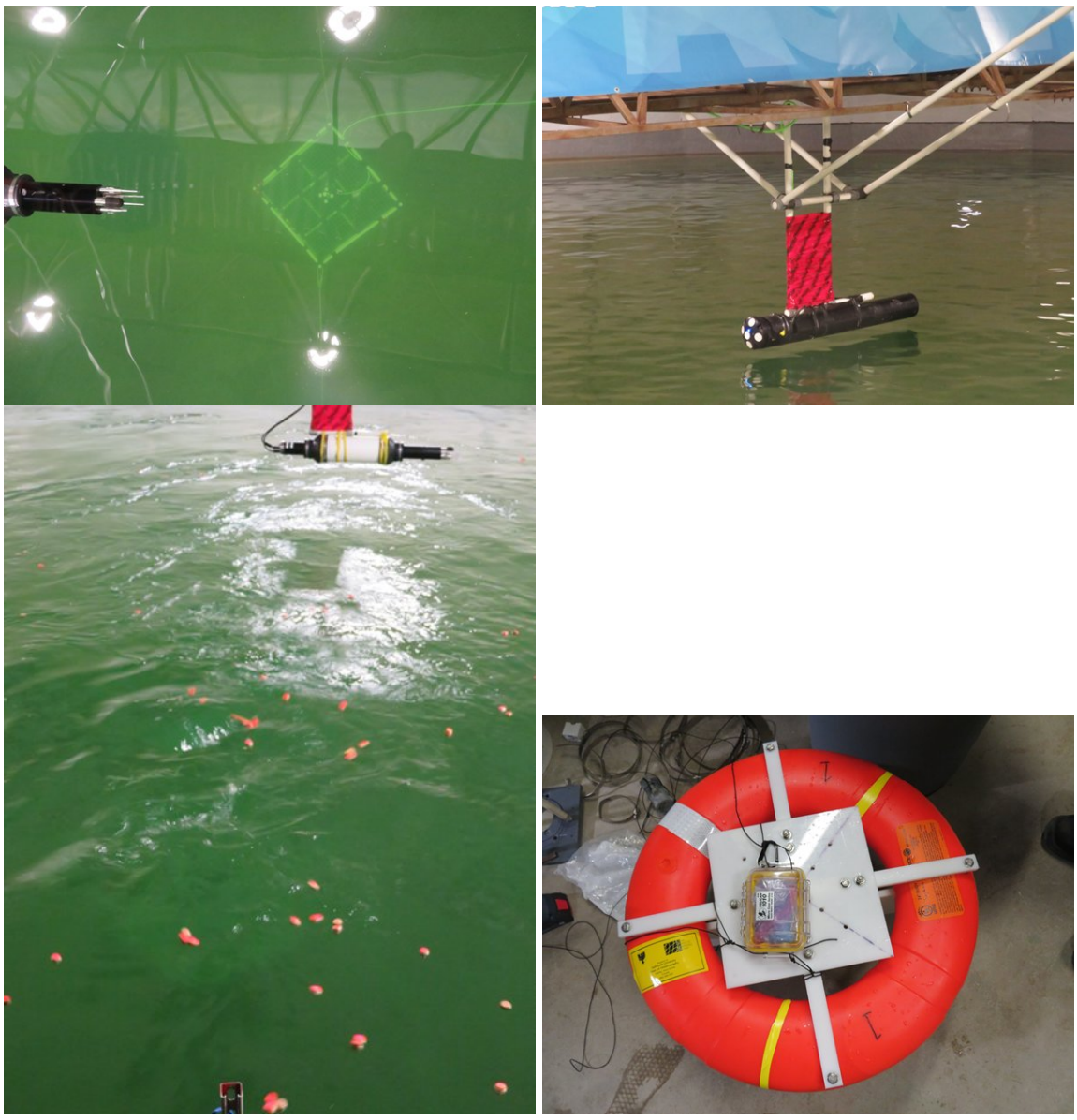

Figure 3: Top Left: Photograph, taken from the bridge, of the rectangular ADCP frame on the bottom of the pool tank. The Signature 1000 is in the centre of the frame. Top Right: Signature1000, in the horizontal configuration. Bottom Left: the corks. Bottom Right: the vorticity drifter, showing the 9-axis inertial motion unit in its watertight container.

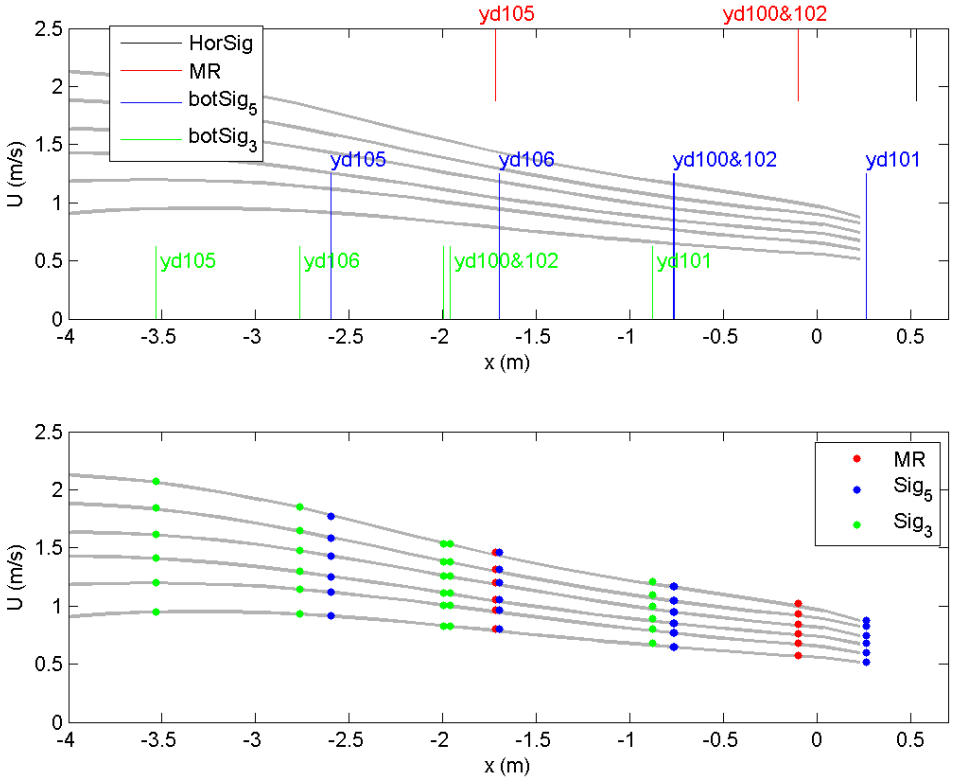

Figure 4: Top Panel: Axial velocity profiles (gray lines) measured with the horizontal ADCP on yd101, and instrument positions on the different days of the experiment. The x-axis is the distance from initial position of the MicroRider endcap. The colours indicate the different instruments. Note that beam 3 and 5 positions correspond to the range bin closest to the MicroRider depth. Bottom Panel: The axial velocity profiles again, with colored dots indicating the values of U at the different instrument positions. The $x = 0$ position corresponds to the MicroRider end cap.

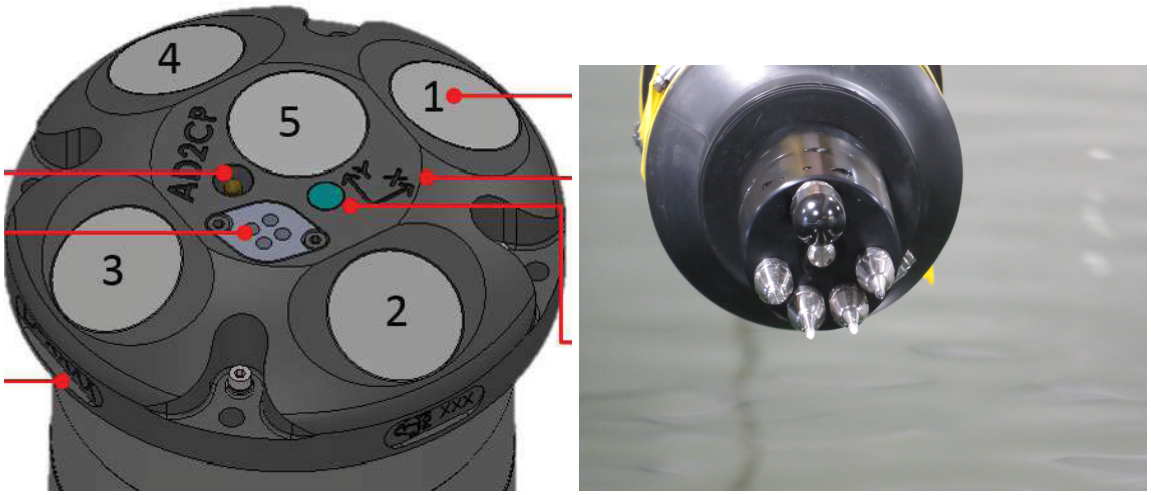

Figure 5: Left panel: sketch of the Signature1000 transducer assembly. Right panel: photograph of the MicroRider sensors. The two shear probes are side-by-side at the bottom. The electromagnetic flow meter is at the top.

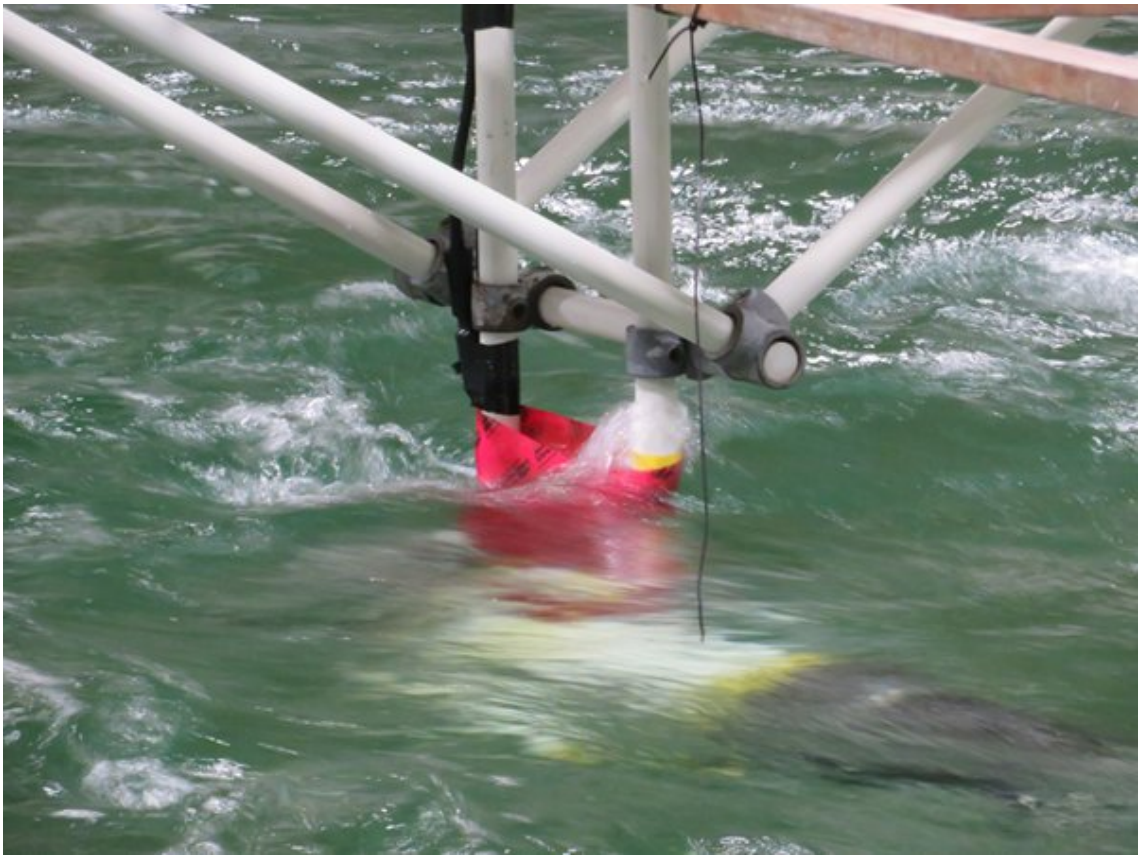

Figure 6: MicroRider in high flow (discharge 100%).

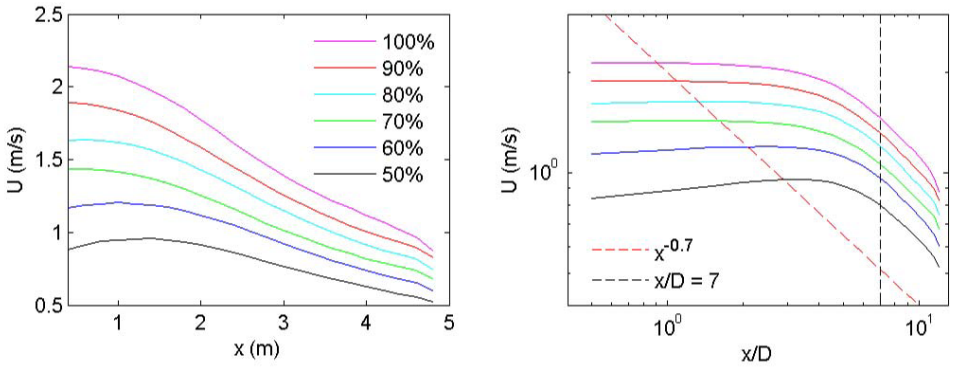

Figure 7: U as a function of discharge percentage and distance from the nozzle in both linear and loglog form (with x normalized by nozzle diameter, D). The dashed lines in the panel at right indicate the expected zone of flow establishment for a cylindrical jet, nominally $x/D \simeq 7$, and the $x^{-0.7}$ dependence expected in the far-field of a round jet confined by a lateral boundary (the water surface in this case).

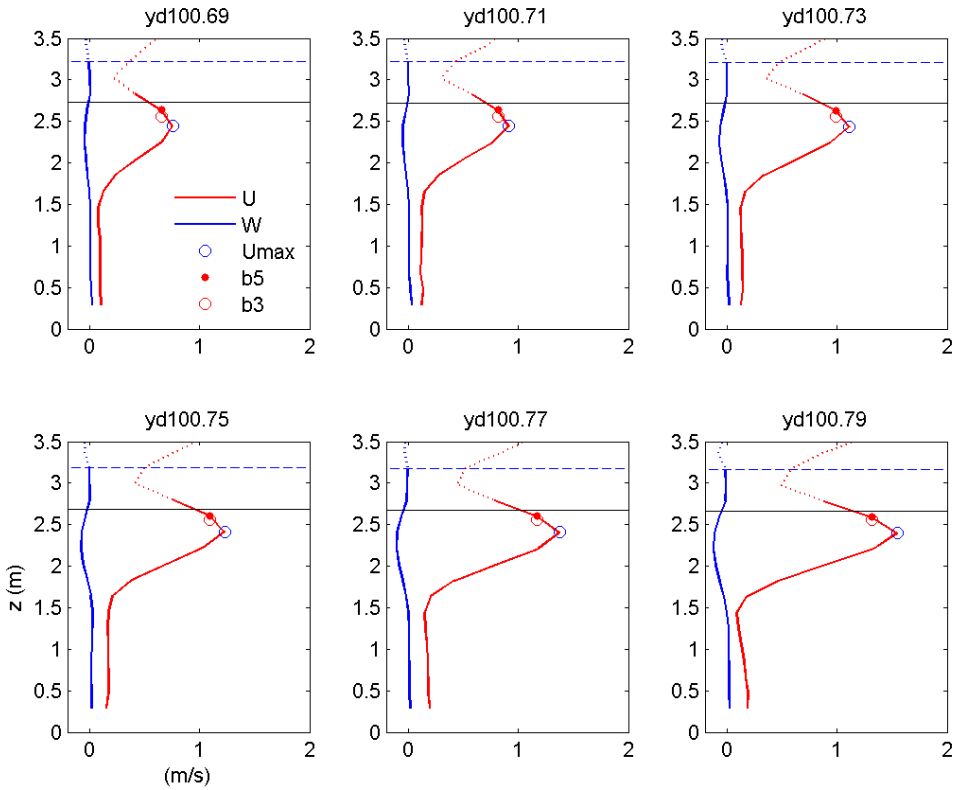

Figure 8: Vertical profiles of horizontal (red) and vertical (blue) velocity from the bottom-mounted ADCP on yd100. Solid lines indicate the reliable sections of the profiles (see text). Starting at the upper left, the discharge increases from 50 to 100% in increments of 10% from left to right in the top and bottom rows. The dashed and solid horizontal lines indicate the water surface and the depth of the MicroRider, respectively. The blue circle is the velocity maximum. The red dot and red circle indicate the range bins closest to the depth of the MicroRider for beams 5 and 3 respectively. (yd100)

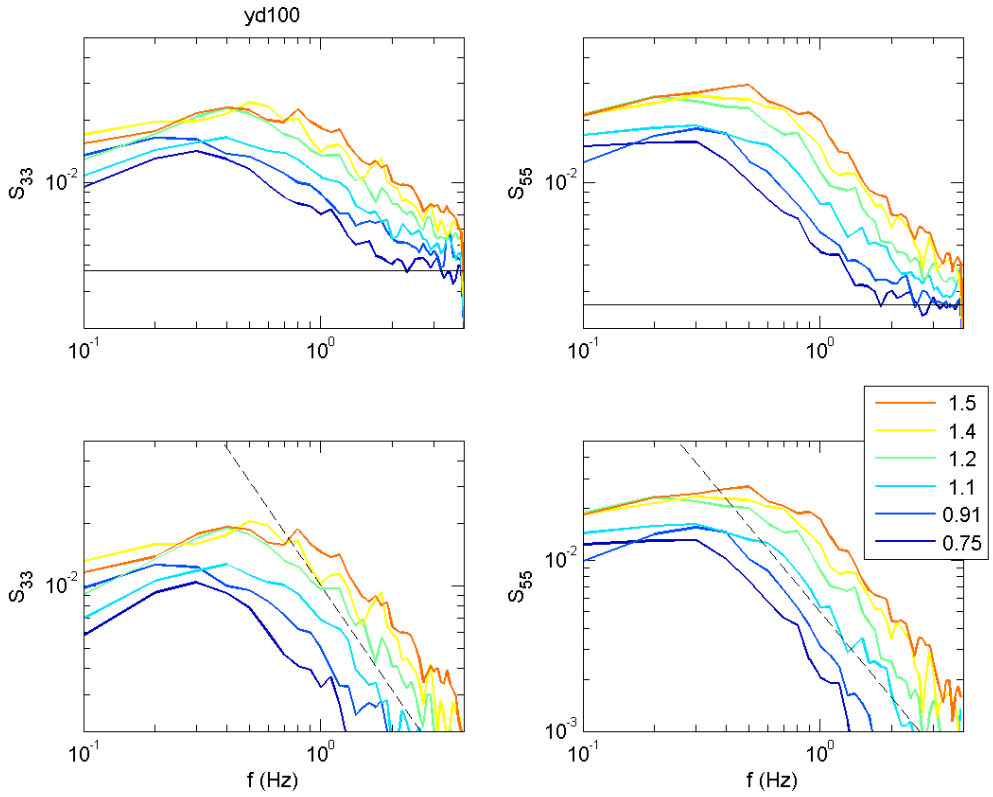

Figure 9: Velocity spectra at the velocity maximum (Fig. 8) for beam 3 (left panels) and beam 5 (right). The grey lines in the top panels indicate the noise levels. This noise has been removed from the spectra in the bottom panels. The dashed line is the expected -5/3 slope in the inertial subrange. (yd100)

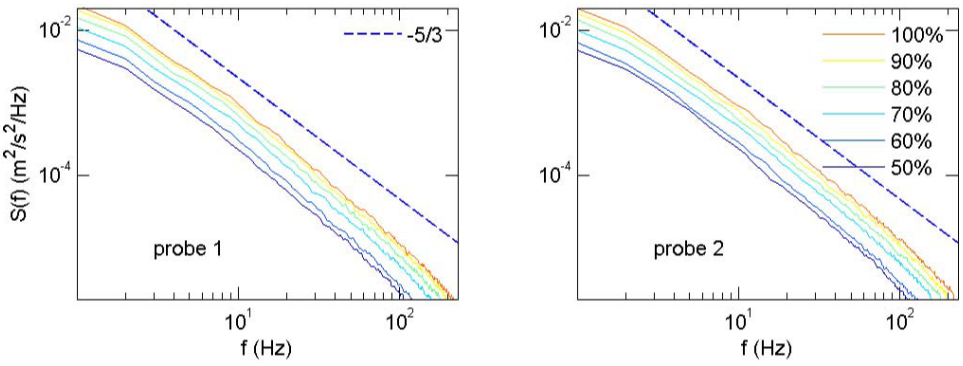

Figure 10: MicroRider velocity spectra. The dashed line is the expected -5/3 slope in the inertial subrange. Colours correspond to the discharge values indicated in the legend. The data correspond to the runs at the MicroRider position on yd105 (Table 1, Fig. 4).

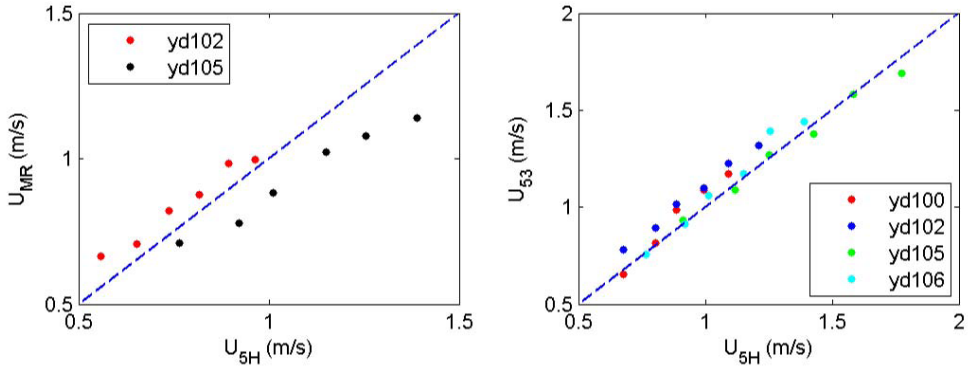

Figure 11: Mean speed comparison. Left panel: U from the electromagnetic flowmeter on the Microrider vs. U from beam 5 of the horizontal ADCP. Note the inconsistent offset from the 1:1 line, and the non-linear behaviour, with the EM flowmeter values trending higher at low flow and lower at high flow. Right panel: U from beams 3 and 5 of the bottom-mounted ADCP vs. U from beam 5 of the horizontal ADCP. Note the linear behaviour, and close adherence to the 1:1 line, compared to the left panel.

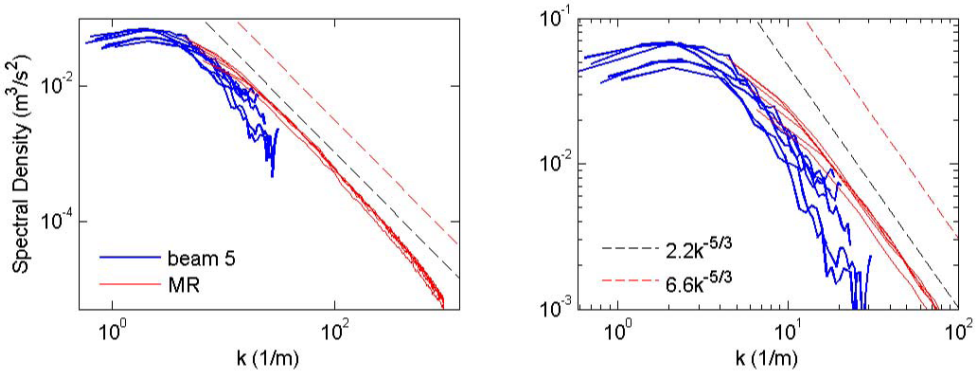

Figure 12: MicroRider and ADCP beam 5 cyclic wavenumber spectra for the six discharge values at $x = -1.7$ m (Table 1). The right panel is an expanded view of the wavenumber range where the two sets of spectra overlap. Note the factor of 3 difference between the -5/3 lines.

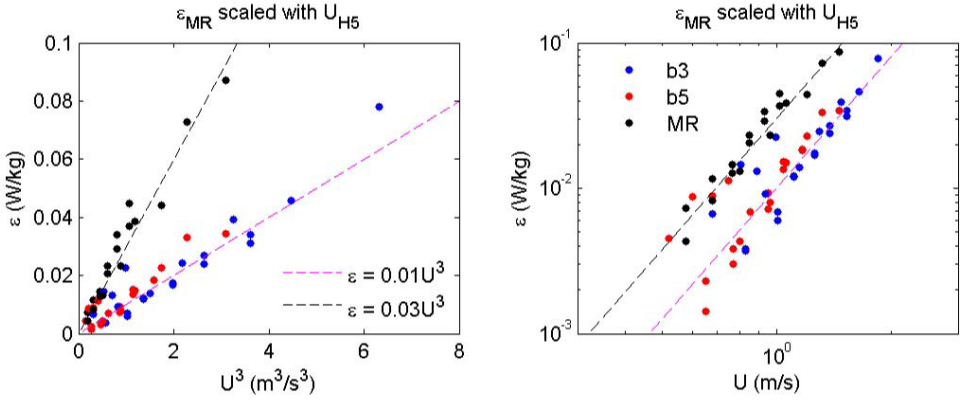

Figure 13: Comparison between the dissipation estimates from the MicroRider shear probes and ADCP beam velocities. Note the expected U^3 dependence exhibited by the three data sets. The shear probe estimates are higher than those from the ADCP by a factor of 3. For both the MicroRider and the ADCP, ϵ was estimated from the spectral densities in the inertial subrange scaled by U from the horizontal ADCP. See text for discussion.

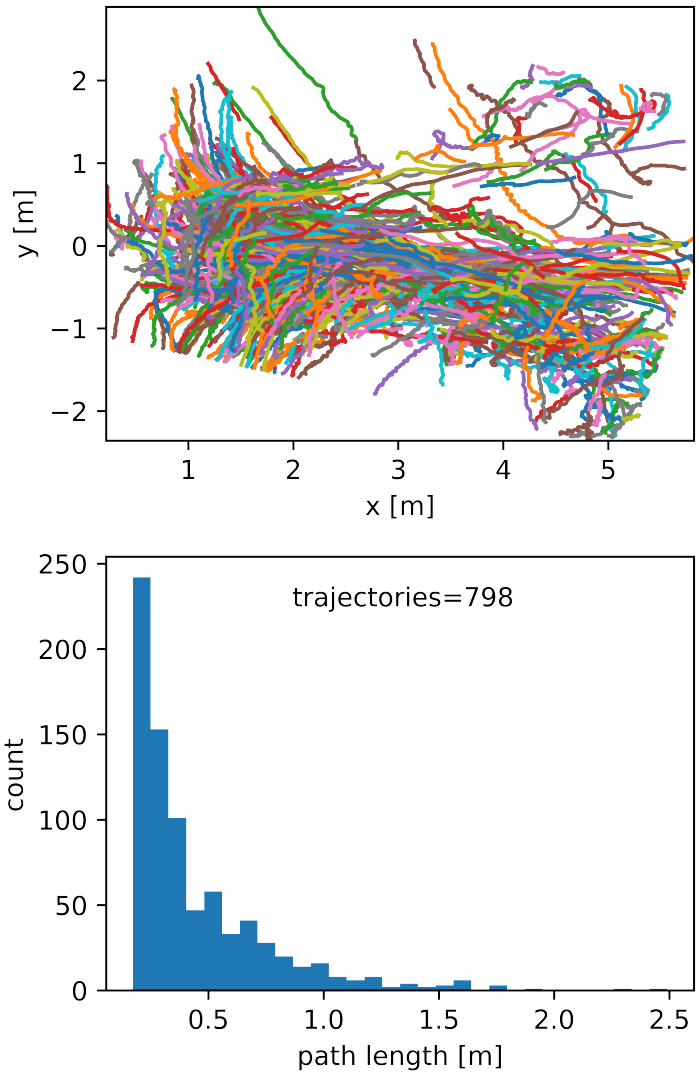

Figure 14: Top panel: composite of all cork trajectories at 100% discharge. Bottom panel: histogram of the trajectory lengths. The nozzle is located at $(x, y) = (0, 0)$.

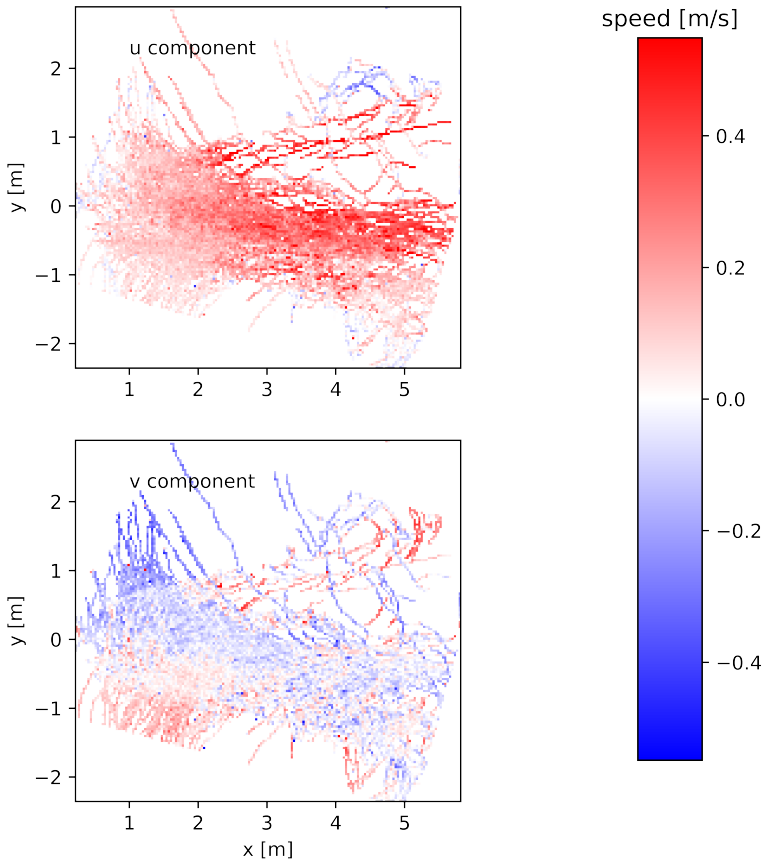

Figure 15: Mean velocities from the trajectories in Fig. 14. Top panel: axial velocity, u. Bottom panel: transverse velocity, v. The nozzle is located at $(x, y) = (0, 0)$. Note the convergence zone for $x < 3$ m, indicated by the change in sign of $\overline{v}$ on either side of $y = 0$, in contrast to $x > 4$ m, where the values $\overline{v}$ exhibit no spatially consistent pattern. These different behaviours are due to horizontal entrainment of surface water into the jet in the zone of flow development, and the dominant role of turbulence in the far-field. Note that results are based on video footage acquired for multiple cork deployments 10 to 15 minutes apart, while the discharge was held constant. The jet axis swings side-to-side on this time scale, a consequence of shear instability coupled to the tank recirculation. The trajectories in the upper right corner that "appear" to leave the jet are a result of such a shift. Discharge 100%.

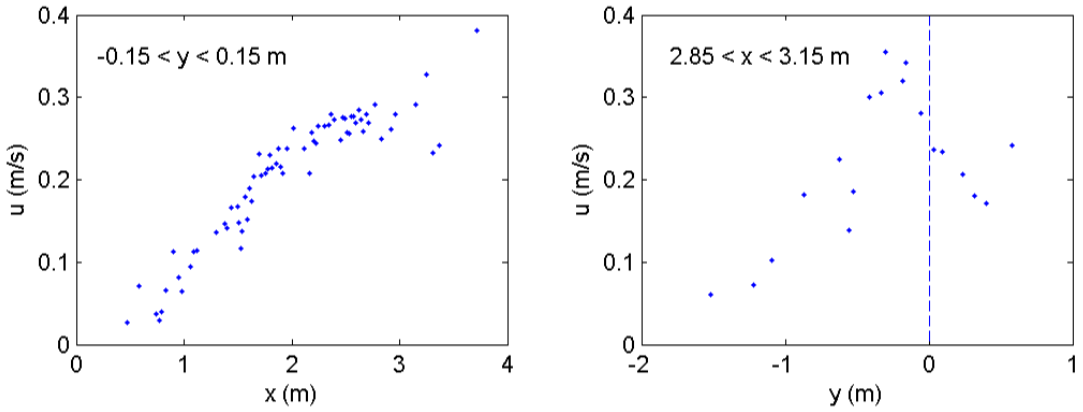

Figure 16: Mean axial velocities from the cork trajectories. Left panel: along the jet ($y = 0$) axis. Right panel: transverse to the jet axis, at $x = 3$ m.

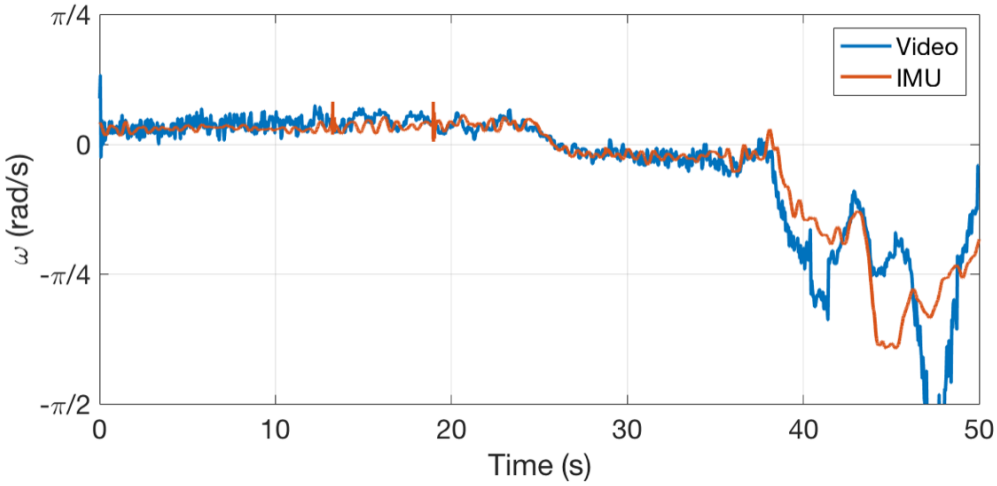

Figure 17: Time series of vorticity along a track followed by the Vorticity Drifter, determined from the rotation rates registered by the 9-axis inertial motion unit (red curve) and estimated from the video imagery (blue curve).